NANOSYSTEMS: PHYSICS, CHEMISTRY, MATHEMATICS, 2018, 9 (3), P. 410–416

On an adsorption/photocatalytic performance of nanotubular $Mg_3Si_2O_5(OH)_4/TiO_2$ composite

A. A. Krasilin[1,2], I. S. Bodalyov[3], A. A. Malkov[3], E. K. Khrapova[2], T. P. Maslennikova[4], A. A. Malygin[3]

[1]Kurnakov Institute of General and Inorganic Chemistry of the Russian Academy of Sciences, 31 Leninsky prospect, Moscow 119991, Russia

[2]Ioffe Institute, 26 Politekhnicheskaya street, St. Petersburg, 194021, Russia

[3]Saint-Petersburg State Institute of Technology, 26 Moskovskiy Prospekt, St. Petersburg 190013, Russia

[4]Institute of Silicate Chemistry, Russian Academy of Sciences, 2 Naberezhnaya Admirala Makarova, St. Petersburg 199034, Russia

ikrasilin@gmail.com

PACS 68.43.Mn, 82.65.+r **DOI 10.17586/2220-8054-2018-9-3-410-416**

Here, we study a performance of nanotubular $Mg_3Si_2O_5(OH)_4/TiO_2$ hybrid adsorbent/photocatalyst in the process of decolorizing an aqueous solution of crystal violet. The composite material was produced by hydrothermal treatment with one or more subsequent cycles of $TiCl_4$ treatment and vapor-phase hydrolysis according to the molecular layering technique. Decolorization was observed in situ by UV-VIS spectroscopy. It was found that TiO_2 deposition yields 2 to 3 times improvement of decolorization performance. Depending on TiO_2 phase type – amorphous or crystalline – this rise is related with either enhancement of adsorption rate either appearance of photocatalytic activity. Finally, fitting procedure issues in case of complex decolorization process were discussed.

Keywords: chrysotile nanotubes, titanium tetrachloride, titanium oxide, crystal violet dye, adsorption, photocatalysis, water remediation.

Received: 1 April 2018

Revised: 8 May 2018

1. Introduction

In the last few decades, wastewater remediation becomes an important problem, the disregard of which accelerates depletion of fresh water resources and ocean contamination. Heavy and textile industries provide various contaminants like heavy metal ions, organic dyes, and diverse organics [1–3]. In order to prevent the overspread of hazardous materials, a number of techniques based on adsorption (separation) [4–7] and catalytic alteration [8–12] can be applied. The problem is that several pollutants can be present in the wastewater simultaneously, and a remediating agent which possesses only one instrument for purification, will not always be capable of handling them simultaneously.

Here, we study a combination of adsorption performance of synthetic $Mg_3Si_2O_5(OH)_4$ chrysotile nanotubes with photocatalytic action of TiO_2. The nanotubes can be synthesized by hydrothermal method using various crystalline and amorphous initial components [13–17]. Flexible capabilities of chemical composition tuning – for example, by introducing various d-elements like Ni [18–20], Co [21], Fe [22–24] – and synthesis conditions allows to control surface properties (active sites) and area [25]. Hydroxyl groups reached surface together with the inner channel make chrysotile nanotubes favorable for adsorption and immobilization of various molecules [26–28] and heavy metal ions of Pb, Cd, Sr, and Nd [29–32].

In turn, TiO_2 is a well-known and widely used photocatalysis for water purification and splitting [33–35]. Its photocatalytic activity can be further enhanced by creating various types of composite materials with metals [12,34], sulfides [36–39], oxides and clays [40–42], or by varying the shape of TiO_2 nanoparticles [43–45]. In our present study, we used molecular layer deposition technique [46, 47] with subsequent hydrolysis to obtain TiO_2 phase on $Mg_3Si_2O_5(OH)_4$ nanotubes.

2. Experimental

Chrysotile nanotubes were synthesized hydrothermally using a procedure described in detail elsewhere [48,49]. Stoichiometric (with Mg:Si molar ratio as 3:2) mixture of MgO and SiO_2 were taken as initial compounds. Hydrothermal treatment was carried out in stainless-steel high-pressure vessels at 350 °C, 70 MPa during 24 h using 1 wt.% NaOH water solution as hydrothermal medium.

$Mg_3Si_2O_5(OH)_4/TiO_2$ composite synthesis was carried by sequential treatment of the nanotubes by $TiCl_4$ and H_2O vapors in a flow-through reactor equipped with a McBain balance (see [49] for details). Initially, as-synthesized nanotubes were annealed at 400 °C for 5 h on air and then exposed to dry N_2 for 2 hours in order to remove adsorbed water molecules and stabilize surface hydroxyl content. On a chemisorption step, chrysotile nanotubes were treated by $TiCl_4$ at 150 °C and 400 °C during 5 – 6 h. Generally, this time is enough to saturate the nanotubes by $TiCl_4$, what was controlled by McBain balance. After that, the reaction zone was purged with dry nitrogen. For the hydrolysis step, the sample was exposed to a stream of air passed at 20 °C through a bubbler filled with distilled water and at temperature in the reactor starting from 150 °C to 400 °C. A final step was purging the reactor with dry N_2 at 400 °C. Four full cycles (chemisorption–purge–hydrolysis–purge) were carried out for the sample treated by $TiCl_4$ at 150 °C in order to increase TiO_2 content.

Thus, 3 samples were prepared for further study: as-synthesized chrysotile nanotubes; nanotubes treated with $TiCl_4$ and H_2O for 4 times (cycles) at the chemisorption temperature of 150 °C; and nanotubes treated once at 400 °C.

X-ray powder diffraction (XRPD) patterns of as-synthesized chrysotile nanotubes and the products of their treatment were acquired by a Rigaku Smartlab SE powder diffractometer with a Cu anode (λ_{Cu}=0.15406 nm) in the 5 – 70 ° 2θ range with 0.01 ° steps A PDF-2 database was used for phase identification and peak indexing.

Specific surface area was calculated involving the Braunauer–Emmett–Teller theory. 9-points N_2 adsorption isotherms were acquired using Micromeritics ASAP 2020 analyzer. Prior the measurement, the samples were annealed at 400° until a constant weight was obtained.

Scanning electron microscopy (SEM) was performed on A Carl Zeiss NVision 40 SEM/EDS workstation.

In situ studies of decolorization performance were carried out on a modular system consisting of a Xe light source (Mikropack HPX-2000), temperature-controlled cuvette holder with magnetic stirrer (Quantum Northwest TC 125), attenuator, optical fiber connectors (Ocean Optics QP600-1-SR), and a UV-VIS spectrometer (Ocean Optics QE 65000). 1.5 ± 0.1 mg of the sample was mixed with 1.9 ml of deionized water in 4 ml PMMA cuvettes. The suspensions obtained were magnetically stirred at 25 °C throughout the experiment. First, the spectrum of each suspension was recorded in the 300 – 800 nm range and stored as the reference. Then, 0.1 ml of 400 mg/l crystal violet aqueous solution was added to the suspension. Absorbance spectra were recorded for every minute during more than 4 hours starting right after the dye addition. Here and subsequently, this regime is called measurement "on light". To exclude action of light, the same batch of kinetics experiment were performed "in dark" by blocking off the beam. The cuvette with the sample was lighted up for 1 – 2 seconds only to acquire the spectra. For 4 hours run, 9 to 10 measurements were made.

Solution decolorization P_t at time t was calculated as follows:

$$P_t = \frac{I_0 - I_t}{I_0} 100\ \%, \tag{1}$$

where I_0 is initial (maximal) absorbance intensity, and I_t is intensity at time t.

3. Results and discussion

Figure 1a shows XRPD patterns of initial sample and its treatment products. According to phase analysis, hydrothermal synthesis yields chrysotile (card #10-381) nanotubes together with some amount of platy lizardite (#82-1837). Principal reflections of chrysotile and lizardite overlap, so only specific lizardite reflections are marked on the XRPD pattern. The presence of the platy lizardite phase could be caused by Al cations presence in starting mixture [48] because Al doping of nanotubular chrysotile strongly effects on its morphology [50]. However, crystallinity of platy lizardite is significantly better than that of tubular chrysotile. The fact that the intensities of reflections at around 35° 2θ are comparable means that the lizardite phase content is negligibly low.

Low-temperature (150 °C) treatment with $TiCl_4$ and H_2O vapors does not lead to formation of new essential crystalline phases except NaCl as a byproduct. Ti element presence with concentration around 0.3 mmol per 1 g of $Mg_3Si_2O_5(OH)_4$ in case of low-temperature treatment was confirmed in [49] by SEM/EDS and chemical analysis, so we can assume that TiO_2 stays mostly in amorphous phase bounded with the chrysotile nanotube surface. High-temperature treatment with $TiCl_4$ and H_2O (400 °C) results in the formation of a mixture of anatase and rutile with predomination of the latter (Ti content around 2.9 mmol/g [49]). Chrysotile phase, in general, withstands the heat exposure, and its XRPD pattern remains the same.

Figure 1b demonstrates specific surface area decrease during the treatment of chrysotile nanotubes with $TiCl_4$ and H_2O vapors. The observable drop is caused both by heat effect (partial chrysotile dehydroxylation and shrinkage of its interlayer space) and, mainly, by mass increase due to $TiCl_4$ deposition and hydrolysis.

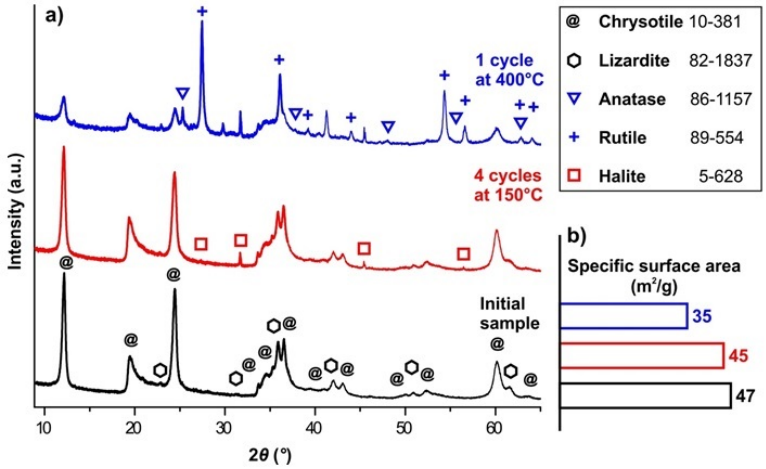

FIG. 1. XRPD patterns of initial sample and samples after treatment with $TiCl_4$ and H_2O vapors (see experimental part for details). Cards numbers are given according to the PDF-2 database; b) Specific (BET) surface area of initial sample and its treatment products

Figure 2 shows SEM-images of the samples obtained in SE (morphological contrast) and BSE modes (phase contrast). As-synthesized chrysotile nanotubes have diameters in the range of 30 – 50 nm and length varying from hundreds of nm up to 1 – 2 μm (Fig. 2a). Chrysotile nanotubes form various morphologies including cylinder, cylinder-in-cylinder, and cone. General nanotubular form preserves during $TiCl_4$ and H_2O vapors treatment, that correlates with the XRPD data. In particular, SEM-images on Fig. 2b (low-temperature treatment) reveal the absence morphology and phase which would differ from the nanotubular one. In contrast, high-temperature treatment (Fig. 2c) leads to the formation of highly crystalline – and more atomically dense in comparison to chrysotile nanotubes – particles which are obviously consist of TiO_2. The average size of the particle is around 100 nm, but there is also a fraction of them with the sizes under tens of nm.

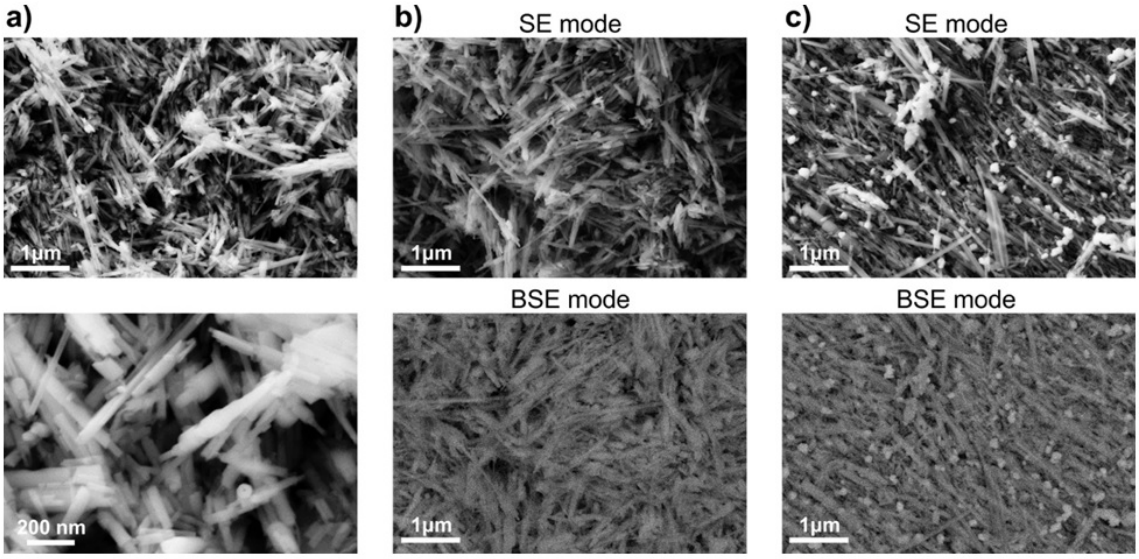

FIG. 2. SEM-images of a) initial sample, b) product of 4 cycles treatment at 150 °C, c) product of 1 cycle treatment at 400 °C. BSE mode gives phase contrast (see text for details)

Figure 3a demonstrates an example of change in crystal violet solution absorbance spectra during $Mg_3Si_2O_5(OH)_4/TiO_2$ composite-promoted decolorization. A common situation for all samples studied is that the majority of the decolorization effect is achieved during the first hour of solution contact with the solid phase. After that time, the decolorization rate decreases gradually. In accordance with Fig. 3, none of the samples was able

to reach 100% decolorization degree, which could be related both with general solid/liquid ratio and the sample's individual performance. And the latter changes drastically.

Comparative analysis of decolorization kinetic curves reveals several following features: 1) decolorization performance of untreated sample (as-synthesized chrysotile nanotubes) is the lowest among the samples tested; 2) there is an increase in decolorization depending on how the measurements were carried out (on light or in dark, see experimental part for details); 3) there is a divergence (at the initial time of the experiment) and then convergence of kinetic curves on Fig. 3c. The initial sample, as we suppose, possesses only adsorption performance, whereas the samples treated by $TiCl_4$ and H_2O vapors can have both adsorption and photocatalytic potential, so it should be primarily compared with the samples investigated in dark. This comparison shows that the chrysotile nanotubes treated by 4 cycles at 150 °C have the highest adsorption performance. Assuming equal measurement conditions (temperature, pH, dye concentration, solid phase mass, stirring), two key factors govern adsorption performance: specific surface area and surface properties. Treatment with $TiCl_4$ and H_2O vapors leads to decrease of the former (Fig. 1b), so the increase of adsorption performance is caused by advantageous change of surface properties, in other words, a number and/or a type (force) of active sites. It is most probably that after low-temperature treatment TiO_2, while it does not form crystalline phase, distributes in an optimal way on the nanotube's surface and forms a large number of active sites, thus increasing total adsorption performance. High-temperature treatment strongly decreases the surface area and forces TiO_2 to form autonomous crystalline phase. Note that the general forms of the kinetic curves on Fig. 3b and Fig. 3d (measured in dark) are highly similar. This fact can be related to partial reduction of chrysotile nanotubes surface properties after crystalline TiO_2 phase formation.

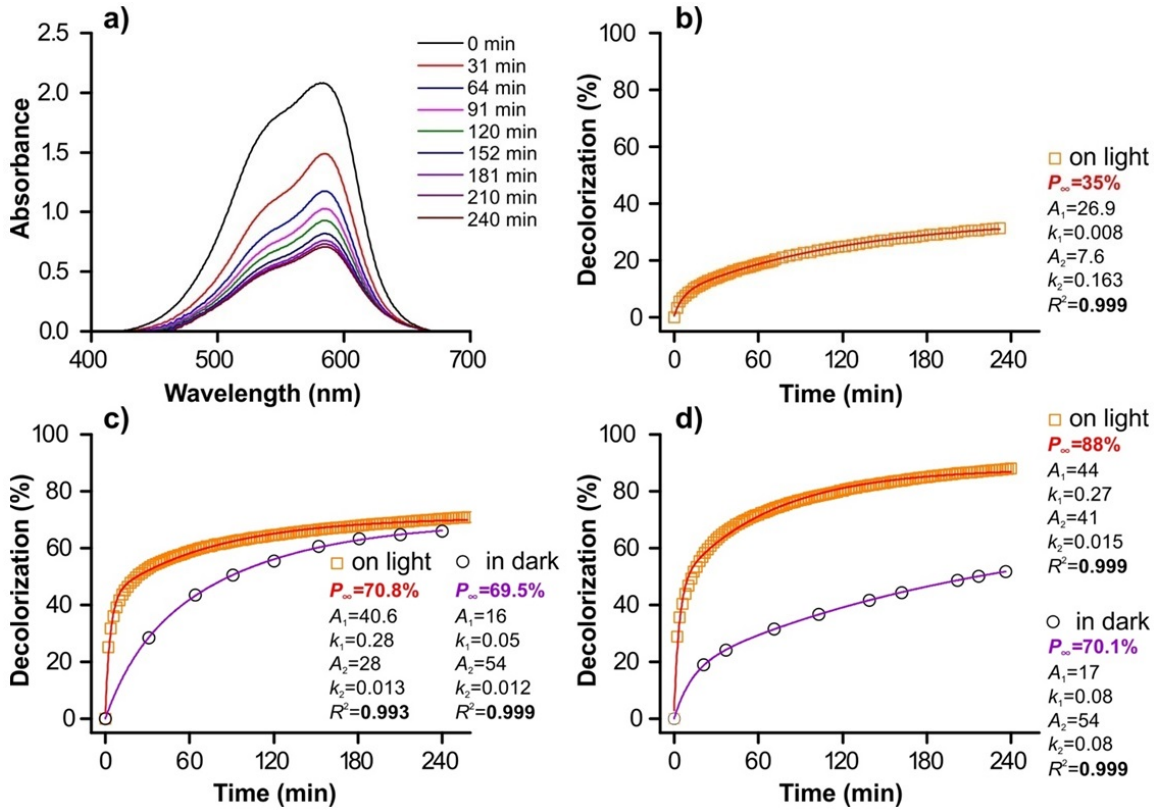

FIG. 3. a) Change in UV-VIS absorbance spectra of crystal violet solution during the decolorization experiment performed in dark (for the 4 treatment cycles at 150 °C). Decolorization curves for b) initial sample, c) sample after 4 treatment cycles at 150 °C, and d) sample after 1 treatment cycle at 400 °C. Points denote experimental data, and solid lines represent the results of fitting procedure (see text for details). Text insets contain information on fitting parameters

The most probable origin of the second feature (Fig. 3c,d) is photocatalytic action of TiO_2. A common condition for the photocatalysis is an existence of sufficiently wide bandgap, which can be realized in crystalline solid. According to that, there is an essential increase of decolorization performance when measured on light

only in case crystalline TiO_2 is present in the system. Interaction with light grants 2 – 3 times increase of decolorization performance (Fig. 3d). After 4 hours of the experiment, the divergence of the curves decreases slightly. In case of amorphous TiO_2 there is also a light-induced decolorization, which can be seen at the very initial time of the process (Fig. 3c), the effect of which vanishes during the experiment. After 4 hours, the two curves become very similar. It is interesting to note that the maximum difference between the curves obtained on light and in dark for both samples achieves after around 15 – 20 minutes of exposure, but crystalline TiO_2 phase provide long-term constant shift of decolorization performance. Most likely this contribution should be related to photocatalytic activity. The $Mg_3Si_2O_5(OH)_4/TiO_2$ composite material obtained by 1 treatment cycle at 400 °C is the most appropriate one in the case of combined adsorption and interaction with light is utilized for water remediation. Considering complex interaction process of pollutant with decontaminating agent, there is often a problem of choosing the appropriate kinetic model. Here, we tried to adopt so-called double-exponential model used for description of heavy metal ions adsorption kinetics [51, 52]. The main reason for the use of this model is that it accounts for two ongoing processes, which, in our case, are adsorption and light-induced decolorization. Model equation is written as follows:

$$P_t = P_\infty - A_1 \exp(-k_1 t) - A_2 \exp(-k_2 t), \tag{2}$$

where P_t is decolorization at time t, P_∞ is decolorization at infinitely long time of the experiment, A_1, k_1, A_2, k_2 are model parameters. The main objective of this fit is to estimate the P_∞ value which determines the performance of the studied material. Nonlinear fitting procedure was applied.

Text insets on Fig. 3b,c,d demonstrate fitting results for the decolorization curves. All cases show high value of adjacent R^2 criterion, which is, does not speak well for applicability and physical consistency of the chosen model. However, we can consider a number of features regarding P_∞ value obtained.

First, for some samples (measured on light) the P_∞ value can be underestimated by the fitting procedure. This is a typical situation for the case of kinetic data approximation [53]. In our case, it especially can be seen on Fig. 3d: there is deviation of the fitted curve at the end of the experiment. In addition, adsorption phenomena are considered to be equilibrium processes (in terms of adsorption and desorption speeds), whereas photocatalysis either occurs continuously either fades out because of photocatalyst degradation, and this can bring additional error to the P_∞ value.

Second, double-exponential model was originally applied solely to the adsorption process, and the parts of the model equation (2) were rather related to certain adsorption stages. This complicates discussion of model parameter values in the case when adsorption is combined with other types of processes promoting decolorization. Nevertheless, we should note the proximity of model parameters for the samples obtained by low- and high-temperature treatment and measured in dark (Fig. 3c,d): treatment regime influences on adsorption rate stronger than on an adsorption capacity (proportional to observed decolorization). Finally, according to fitting results on Fig. 3d, the light-induced process which granted the highest performance of the composite with crystalline TiO_2 will lose its influence at long-term exposure lying beyond the current experiment time.

4. Conclusion

Here, we report on the application of $Mg_3Si_2O_5(OH)_4$ chrysotile nanotubes / TiO_2 composite as an adsorbent and photocatalyst for the process of decolorization of crystal violet. The composite material was obtained by hydrothermal synthesis of nanotubes with subsequent treatment with $TiCl_4$ and H_2O vapors according to the molecular layering technique. This treatment allows control of the TiO_2 content and phase state. Chrysotile nanotube treatment results in a 2- to 3-fold increase of their decolorization potential, depending on TiO_2 phase type. If it forms amorphous phase on the nanotubes surface, then the increase is caused mostly by favorable change of the active sites type. If it forms crystal phase, then decolorization is a combined action of adsorption and photocatalysis. The latter affords the highest decolorization rates.

Although the proposed composites are promising for the cases where combined remediation action is needed, there is still a number of hindrances regarding quantitative description (modeling) of the overall process kinetics. This is crucial for both in-depth understanding of relations between adsorption and photocatalysis, and design of an appropriate apparatus.

Acknowledgements

The research was supported by Russian Science Foundation grant 17-73-10426.
The SEM research was performed using the equipment of the JRC PMR IGIC RAS. The XRPD study was performed using the equipment of the Engineering Centre of Saint Petersburg State Technological Institute (Technical University).

References

[1] Burakov A.E., Galunin E.V., Burakova I.V., Kucherova A.E., Agarwal S., Tkachev A.G., Gupta V.K. Adsorption of heavy metals on conventional and nanostructured materials for wastewater treatment purposes: A review. *Ecotoxicol. Environ. Saf*., 2018, **148**, P. 702–712.

[2] Khin M.M., Nair A.S., Babu V.J., Murugan R., Ramakrishna S. A review on nanomaterials for environmental remediation. *Energy Environ. Sci*., 2012, **5** (8), P. 8075.

[3] Cai Z., Sun Y., Liu W., Pan F., Sun P., Fu J. An overview of nanomaterials applied for removing dyes from wastewater. *Environ. Sci. Pollut. Res*., 2017, **24** (19), P. 15882–15904.

[4] Ali I., Gupta V.K. Advances in water treatment by adsorption technology. *Nat. Protoc*., 2007, **1** (6), P. 2661–2667.

[5] Kamaruddin M.A., Yusoff M.S., Aziz H.A., Akinbile C.O. Recent developments of textile waste water treatment by adsorption process: a review. *Int. J. Sci. Res. Knowl*, 2013, P. 60–73.

[6] Mittal A., Mittal J., Malviya A., Kaur D., Gupta V.K. Adsorption of hazardous dye crystal violet from wastewater by waste materials. *J. Colloid Interface Sci*., 2010, **343** (2), P. 463–473.

[7] Gupta V.K., Kumar R., Nayak A., Saleh T.A., Barakat M.A. Adsorptive removal of dyes from aqueous solution onto carbon nanotubes: A review. *Adv. Colloid Interface Sci*., 2013, **193–194**, P. 24–34.

[8] Peter A., Mihaly-Cozmuta A., Nicula C., Mihaly-Cozmuta L., Jastrzbska A., Olszyna A., Baia L. UV light-assisted degradation of methyl orange, methylene blue, phenol, salicylic acid, and rhodamine B: photolysis versus photocatalyis. *Water, Air, Soil Pollut.*, 2017, **228** (1), P. 41.

[9] Mohmood I., Lopes C.B., Lopes I., Ahmad I., Duarte A.C., Pereira E. Nanoscale materials and their use in water contaminants removal – a review. *Environ. Sci. Pollut. Re*s., 2013, **20** (3), P. 1239–1260.

[10] Chakma S., Moholkar V.S. Investigation in mechanistic issues of sonocatalysis and sonophotocatalysis using pure and doped photocatalysts. *Ultrason. Sonochem.*, 2015, **22**, P. 287–299.

[11] Chu K.H., Al-Hamadani Y.A.J., Park C.M., Lee G., Jang M., Jang A., Her N., Son A., Yoon Y. Ultrasonic treatment of endocrine disrupting compounds, pharmaceuticals, and personal care products in water: A review. *Chem. Eng. J.*, 2017, **327**, P. 629–647.

[12] Kozlov D.A., Lebedev V.A., Polyakov A.Y., Khazova K.M., Garshev A.V. The microstructure effect on the Au/TiO_2 and Ag/TiO_2 nanocomposites photocatalytic activity. *Nanosyst.: Phys. Chem. Math.*, 2018, **9** (2), P. 266–278.

[13] Korytkova E.N., Maslov A.V., Pivovarova L.N., Drozdova I.A., Gusarov V.V. Formation of $Mg_3Si_2O_5(OH)_4$ nanotubes under hydrothermal conditions. *Glas. Phys. Chem*., 2004, **30** (1), P. 51–55.

[14] Falini G., Foresti E., Gazzano M., Gualtieri A.F., Leoni M., Lesci I.G., Roveri N. Tubular-shaped stoichiometric chrysotile nanocrystals. *Chem. Eur. J.*, 2004, **10** (12), P. 3043–3049.

[15] Bloise A., Belluso E., Catalano M., Barrese E., Miriello D., Apollaro C. Hydrothermal alteration of glass to chrysotile. *J. Am. Ceram. Soc.*, 2012, **95** (10), P. 3050–3055.

[16] Lafay R., Montes-Hernandez G., Janots E., Chiriac R., Findling N., Toche F. Nucleation and growth of chrysotile nanotubes in $H_2SiO_3/MgCl_2$/NaOH medium at 90 to 300 °C. *Chem. Eur. J*., 2013, **19** (17), P. 5417–5424.

[17] Krasilin A.A., Nevedomsky V.N., Gusarov V.V. Comparative energy modeling of multiwalled $Mg_3Si_2O_5(OH)_4$ and $Ni_3Si_2O_5(OH)_4$ nanoscroll growth. *J. Phys. Chem. C*., 2017, **121** (22), P. 12495–12502.

[18] Bloise A., Belluso E., Fornero E., Rinaudo C., Barrese E., Capella S. Influence of synthesis conditions on growth of Ni-doped chrysotile. *Microp. Mesop. Mater*., 2010, **132** (1–2), P. 239–245.

[19] McDonald A., Scott B., Villemure G. Hydrothermal preparation of nanotubular particles of a 1:1 nickel phyllosilicate. *Microp. Mesop. Mater*., 2009, **120** (3), P. 263–266.

[20] Krasilin A.A., Gusarov V.V. Redistribution of Mg and Ni cations in crystal lattice of conical nanotube with chrysotile structure. *Nanosyst.: Phys. Chem. Math*., 2017, **8** (5), P. 620–627.

[21] Korytkova E.N., Pivovarova L.N. Hydrothermal synthesis of nanotubes based on $(Mg,Fe,Co,Ni)_3Si_2O_5(OH)_4$ hydrosilicates. *Glas. Phys. Chem*., 2010, **36** (1), P. 53–60.

[22] Piperno S. et al. Characterization of geoinspired and synthetic chrysotile nanotubes by atomic force microscopy and transmission electron microscopy. *Adv. Funct. Mater*., 2007, **17** (16), P. 3332–3338.

[23] Korytkova E.N., Pivovarova L.N., Semenova O.E., Drozdova I.A., Povinich V.F., Gusarov V.V. Hydrothermal synthesis of nanotubular Mg-Fe hydrosilicate. *Russ. J. Inorg. Chem*., 2007, **52** (3), P. 338–344.

[24] Krasilin A.A., Panchuk V.V., Semenov V.G., Gusarov V.V. Formation of variable-composition iron(III) hydrosilicates with the chrysotile structure. *Russ. J. Gen. Chem*., 2016, **86** (12), P. 2581-2588.

[25] White R.D., Bavykin D. V, Walsh F.C. Morphological control of synthetic $Ni_3Si_2O_5(OH)_4$ nanotubes in an alkaline hydrothermal environment. *J. Mater. Chem. A*., 2013, **1** (3), P. 548–556.

[26] Artali R., Del Pra A., Foresti E., Lesci I.G., Roveri N., Sabatino P. Adsorption of human serum albumin on the chrysotile surface: a molecular dynamics and spectroscopic investigation. *J. R. Soc. Interface*, 2008, **5** (20), P. 273–283.

[27] Valentim I.B., Joekes I. Adsorption of sodium dodecylsulfate on chrysotile. *Coll. Surf., A: Physicochem., Eng. Aspects*, 2006, **290** (1–3), P. 106–111.

[28] Teixeira A.P.C., Purceno A.D., de Paula C.C.A., da Silva J.C.C., Ardisson J.D., Lago R.M. Efficient and versatile fibrous adsorbent based on magnetic amphiphilic composites of chrysotile/carbon nanostructures for the removal of ethynilestradiol. *J. Hazard. Mater*., 2013, **248–249**, P. 295–302.

[29] Cheng L.L., Wei X.D., Hao X.L., Ruan D., Yu S.M. The removal of strontium(II) and neodymium(III) from their aqueous solutions on chrysotile nanotubes. *Adv. Mater. Res*., 2014, **881–883**, P. 519–524.

[30] Yu S., Zhai L., Wang Y., Liu X., Xu L., Cheng L. Synthesis of magnetic chrysotile nanotubes for adsorption of Pb(II), Cd(II) and Cr(III) ions from aqueous solution. *J. Environ. Chem. Eng.*, 2015, **3** (2), 752–762.

[31] Cheng L., Ren X., Wei X., Sun X., Yu S. Facile synthesis and characterization of chrysotile nanotubes and their application for lead(II) removal from aqueous solution. *Sep. Sci. Technol*., 2014, **50** (5), P. 700–709.

[32] Golubeva O.Y., Maslennikova T.P., Ulyanova N.Y., Dyakina M.P. Sorption of lead(II) ions and water vapors by synthetic hydro- and aluminosilicates with layered, framework, and nanotube morphology. *Glas. Phys. Chem.*, 2014, **40** (2), P. 250–255.

[33] Chong M.N., Jin B., Chow C.W.K., Saint C. Recent developments in photocatalytic water treatment technology: A review. *Water Res*., 2010, **44** (10), P. 2997–3027.
[34] Karthikeyan N., Narayanan V., Stephen A. Visible light degradation of textile effluent using nanostructured TiO_2/Ag/CuO photocatalysts. *Nanosyst.: Phys. Chem. Math.*, 2016, **7** (4), P. 695–698.
[35] Subramanian V.R., Sarker S., Yu B., Kar A., Sun X., Dey S.K. TiO_2 nanotubes and its composites: Photocatalytic and other photo-driven applications. *J. Mater. Res.*, 2013, **28** (3), P. 280–293.
[36] Zhukovskiy M.A., Smirnova N.P., Rusetsky I.A., Kolbasov G.Y., Eremenko A.M. Physical and chemical properties and photocatalytic activity of nanostructured TiO_2/CdS Films. *J. Appl. Spectrosc.*, 2014, **81** (2), P. 238–243.
[37] Kozlova E.A., Kozhevnikova N.S., Cherepanova S.V., Lyubina T.P., Gerasimov E.Y., Kaichev V.V., Vorontsov A.V., Tsybulya S.V., Rempel A.A., Parmon V.N. Photocatalytic oxidation of ethanol vapors under visible light on CdS–TiO_2 nanocatalyst. *J. Photochem. Photobiol. A Chem.*, 2012, **250**, P. 103–109.
[38] Kozlova E.A., Rempel' A.A., Valeeva A.A., Gorbunova T.I., Kozhevnikova N.S., Cherepanova S.V., Gerasimov E.Yu., Saraev A.A., Korovin E.Yu., Parmon V.N. Photoactivity of TiO_2/CdS and SiO_2/CdS hybrid nanostructured systems in the partial oxidation of ethanol under irradiation with visible light. *Kinet. Catal.*, 2015, **56** (4), P. 515–522.
[39] Zheng L., Han S., Liu H., Yu P., Fang X. Hierarchical MoS_2 nanosheet@TiO_2 nanotube array composites with enhanced photocatalytic and photocurrent performances. *Small*, 2016, **12** (11), P. 1527–1536.
[40] Chen J.-Z., Chen T.-H., Lai L.-W., Li P.-Y., Liu H.-W., Hong Y.-Y., Liu D.-S. Preparation and characterization of surface photocatalytic activity with NiO/TiO_2 nanocomposite structure. *Materials (Basel)*, 2015, **8** (7), P. 4273–4286.
[41] Wang Y.-F., Hsieh M.-C., Lee J.-F., Yang C.-M. Nonaqueous synthesis of CoO_x/TiO_2 nanocomposites showing high photocatalytic activity of hydrogen generation. *Appl. Catal. B Environ*., 2013, **142**, P. 626–632.
[42] Szczepanik B. Photocatalytic degradation of organic contaminants over clay-TiO_2 nanocomposites: A review. *Appl. Clay Sci*., 2017, **141**, P. 227–239.
[43] Maksimov V.D., Shaporev A.S., Ivanov V.K., Churagulov B.R., Tret'yakov Y.D. Hydrothermal synthesis of nanocrystalline anatase from aqueous solutions of titanyl sulfate for photocatalytic applications. *Theor. Found. Chem. Eng.*, 2009, **43** (5), P. 713–718.
[44] Meskin P.E., Gavrilov A.I., Maksimov V.D., Ivanov V.K., Churagulov B.P. Hydrothermal/microwave and hydrothermal/ultrasonic synthesis of nanocrystalline titania, zirconia, and hafnia. *Russ. J. Inorg. Chem.*, 2007, **52** (11), P. 1648–1656.
[45] Sadovnikov A.A., Baranchikov A.E., Zubavichus Y.V., Ivanova O.S., Murzin V.Y., Kozik V.V., Ivanov V.K. Photocatalytically active fluorinated nano-titania synthesized by microwave-assisted hydrothermal treatment. *J. Photochem. Photobiol. A Chem.*, 2015, **303**, P. 36–43.
[46] Malygin A.A., Malkov A.A., Sosnov E.A. Structural-dimensional effects and their application in the "core–nanoshell" systems synthesized by molecular layering. *Russ. Chem. Bull., Int. Ed.*, 2017, **66** (11), P. 1939–1962.
[47] Abdulagatov A.I., Hall R.A., Sutherland J.L., Lee B.H., Cavanagh A.S., George S.M. Molecular layer deposition of titanicone films using $TiCl_4$ and ethylene glycol or glycerol: growth and properties. *Chem. Mater.*, 2012, **24** (15), P. 2854–2863.
[48] Maslennikova T.P., Korytkova E.N. Regularities of the filling of $Mg_3Si_2O_5(OH)_4$ hydrosilicate nanotubes with solutions of sodium hydroxide and sodium chloride. *Glas. Phys. Chem.*, 2011, **37** (4), P. 418–425.
[49] Bodalyov I.S., Malkov A.A., Korytkova E.N., Maslennikova T.P., Malygin A.A. Temperature factor in interaction of nanotubular magnesium hydrosilicate, $Mg_3Si_2O_5(OH)_4$, with titanium tetrachloride and water vapors. *Russ. J. Appl. Chem.*, 2014, **87** (2), P. 151–159.
[50] Krasilin A.A., Gusarov V.V. Control over morphology of magnesium-aluminum hydrosilicate nanoscrolls. *Russ. J. Appl. Chem.*, 2015, **88** (12), P. 1928–1935.
[51] Chiron N., Guilet R., Deydier E. Adsorption of Cu(II) and Pb(II) onto a grafted silica: isotherms and kinetic models. *Water Res.*, 2003, **37** (13), P. 3079–3086.
[52] Wilczak A., Keinath T.M. Kinetics of sorption and desorption of copper(II) and lead (II) on activated carbon. *Water Environ. Res.*, 1993, **65** (3), P. 238–244.
[53] Plazinski W., Rudzinski W., Plazinska A. Theoretical models of sorption kinetics including a surface reaction mechanism: A review. *Adv. Colloid Interface Sci*., 2009, **152** (1-2), P. 2–13.